Research Square

Preprints are preliminary reports that have not undergone peer review.
They should not be considered conclusive, used to inform clinical practice,
or referenced by the media as validated information.

Spatial and functional heterogeneity of CAFs at the tumor center and infiltrating front of OSCC with distinct WPOI Patterns

TING ZHOUT
Nanjing University
xiaoxin zhang
6932163710qq.com

Nanjing University
Yanhong Ni
Nanjing University
qingang Hu
Nanjing University
Lei zhang
Nanjing University

Article

Keywords: CAFs, WPOI, Tumor center, Invasive tumor front, Oral squamous cell carcinoma

Posted Date: November 12th, 2026

DOI: https://doi.org/10.21203/rs.3.rs-10837722/v1

License: This work is licensed under a Creative Commons Attribution 4.0 International License.
Read Full License

Additional Declarations: No competing interests reported.

Spatial and functional heterogeneity of CAFs at the tumor center and infiltrating front of OSCC with distinct WPOI Patterns

Ting Zhou [1], Xiaoxin Zhang [2], Yanhong Ni [2], Qingang Hu [1*] Lei Zhang [3*]

1 Department of Oral-maxillofacial surgery, Nanjing Stomatological Hospital, Affiliated Hospital of Medical School, Research Institute of Stomatology, Nanjing University, Nanjing, China, 210008

2 Central Laboratory of Stomatology, Nanjing Stomatological Hospital, Affiliated Hospital of Medical School, Research Institute of Stomatology, Nanjing University, Nanjing, China, 210008

3 Department of Oral Pathology, Nanjing Stomatological Hospital, Affiliated Hospital of Medical School, Research Institute of Stomatology, Nanjing University, Nanjing, China, 210008

*Correspondence: 249486723@qq.com, qghu@nju.edu.cn

Abstract

Background: The worst pattern of invasion (WPOI) is an established prognostic determinant in oral squamous cell carcinoma (OSCC), yet the stromal mechanisms underlying the highly invasive WPOI4–5 pattern remain poorly defined. Cancer-associated fibroblasts (CAFs) are implicated in tumor invasion and involved in WPOI formation, but the presence and the function of CAFs at the tumor center (TC) and invasive tumor front (ITF) contribute equally were unknown.

Methods: We performed α-SMA immunohistochemistry on 137 OSCC specimens (59 WPOI1–3, 78 WPOI4–5) and correlated IHC score of α-SMA in CAFs at the TC and ITF with clinicopathologic features and overall survival. Paired CAFs derived from both regions of WPOI1–3 and WPOI4–5 tumors were subjected to RNA sequencing and in vitro proliferation, migration, and tumor-cell co-culture assays were performed.

Results: α-SMA IHC score CAFs was higher within the ITF relative to the TC in both WPOI groups, and this front-to-center gradient was significantly amplified in WPOI4–5 patients (interaction $P = 0.0089$). ITF, but not TC, α-SMA expression in CAFs was associated with WPOI4–5 ($P < 0.001$), whereas high α-SMA expression at both locations predicted shorter overall survival in WPOI4–5 tumors. Transcriptomic analysis revealed that WPOI4–5 ITF CAFs undergo a shift toward inflammatory, secretory, and extracellular-matrix-remodeling programs, with a negative enrichment of proliferative and metabolic pathways. Functionally, WPOI4–5 ITF derived CAFs exhibited the highest migratory capacity and the strongest pro-migratory effect on

OSCC cells in vitro, despite a globally elevated proliferative potential of WPOI4–5 CAFs irrespective of region.

Conclusions: CAFs in WPOI4–5 OSCC are functionally distinct from those in WPOI1–3 tumors, with the most pronounced pro-invasive properties at the ITF. These findings identify ITF CAFs as a candidate stromal driver of the WPOI4–5 phenotype and a potential therapeutic target in highly invasive OSCC.

Key words: CAFs; WPOI; Tumor center;Invasive tumor front; Oral squamous cell carcinoma;

Introduction

Oral squamous cell carcinoma (OSCC) is the most common malignancy of the head and neck, with a five-year overall survival that has remained at 50–60% for decades despite advances in treatment[1]. Established prognostic factors—including HPV status, TP53 mutation, and histologic differentiation—only partially account for the variability in clinical outcomes[2-4], underscoring the need to identify additional determinants of tumor aggressiveness.

The worst pattern of invasion (WPOI) has emerged as one such determinant. WPOI describes the manner in which tumor cells invade into surrounding tissue at the tumor–host interface and is graded into five patterns[3,5]: WPOI-1, broad pushing borders; WPOI-2, finger-like growth or separate large tumor islands; WPOI-3, invasive islands of more than 15 cells; WPOI-4, small infiltrative nests or cords of ≤15 cells or single-cell infiltration; and WPOI-5, dispersed tumor satellites of any size located ≥1 mm from the main tumor mass. Multiple studies and meta-analyses have established that the highly invasive patterns WPOI4–5 are independently associated with worse survival, higher recurrence, and increased locoregional failure[6,7], and WPOI4–5 has been incorporated into the AJCC 8th edition staging manual as a prognostic marker[8]. However, although $WPOI_{4–5}$ is defined by the presence of dispersed tumor cells at the invasive tumor front (ITF), the biological mechanisms that generate this pattern remain largely unknown.

It is now well established that tumor behavior is shaped not only by cancer cells but also by the surrounding tumor microenvironment, in which cancer-associated fibroblasts (CAFs) are a major stromal component. In OSCC, stromal α-SMA^+ CAF

abundance has been associated with advanced stage, recurrence, and poor prognosis [9-12]. We previously demonstrated that CAFs actively contribute to WPOI4–5 formation through the OXTR–ERK signaling axis[13], providing direct evidence that the stroma participates in shaping the invasive pattern. However, CAFs are increasingly recognized as a heterogeneous population with functionally distinct, and sometimes opposing subtypes[14-16]. Because WPOI is by definition assessed at the ITF, a unresolved question is whether the contribution of CAFs to WPOI4–5 is dictated by their location, specifically whether ITF-resident CAFs are uniquely responsible, or whether CAFs at the tumor center (TC) share the same properties. Distinguishing between these possibilities has direct implications for understanding how WPOI4–5 arises and for identifying the spatial compartment that should be targeted therapeutically.

To address this question, we systematically compared α-SMA expression in CAFs at the TC and ITF between WPOI1–3 and WPOI4–5 tumors, evaluated the clinicopathologic and prognostic significance of α-SMA expression at each location, and isolated CAFs from both regions of WPOI1–3 and WPOI4–5 tumors for transcriptomic profiling and in vitro functional assays. Our results revealed that WPOI4–5 tumors harbored a functionally distinct CAFs population whose malignant properties were most pronounced at the ITF, providing a stromal explanation for the formation and prognostic impact of the WPOI4–5 invasive phenotype.

Material and methods

2.1 Patients and Samples

This study enrolled 137 paraffin-embedded specimens from patients with OSCC treated at Nanjing Stomatological Hospital between 2019 and 2022. Inclusion criteria: (1) patients who underwent surgical treatment without preoperative radiotherapy; (2) availability of adequate tumor tissue containing both the TC and ITF. Exclusion criteria: (1) incomplete clinicopathological data; (2) recurrent cases or those who received preoperative radiotherapy; (3) tumors not originating from the oral and maxillofacial region.

Tumors were stratified into WPOI1–3 (n = 59) and WPOI4–5 (n = 78) groups by two experienced pathologists according to the Brandwein-Gensler criteria[3]. The TC was defined as the central intratumoral region located away from the invasive margin,

whereas the ITF was defined as the deepest advancing margin at which invasive tumor islands, cords or individual tumor cells interfaced with the surrounding stroma. Patient samples and clinical information were acquired with informed consent and approved by the Research Ethics Committee of Nanjing Stomatological Hospital (Approval Number: NJSH-2021NL-26). This study was performed in accordance with the Declaration of Helsinki. Patients were followed for 11–36 months. Overall survival (OS) was defined as the time from surgery to death from any cause.

2.2 Immunohistochemical (IHC) staining

IHC staining for α-SMA was performed according to standard protocols. Staining outcomes were evaluated independently by two experienced pathologists blinded to clinicopathologic data. Staining intensity was graded as: 0, no staining; 1, weak (yellowish); 2, moderate (yellow); 3, strong (brownish yellow). The proportion of positive cells was graded as: 0, <5%; 1, 5–24%; 2, 25–50%; 3, 51–74%; 4, ≥75%. The final IHC score was the product of intensity and proportion grades (range 0–12). For correlation with clinicopathologic parameters and survival analysis, scores were dichotomized into low (<median) and high (≥median) groups.

2.3 CAFs isolation

Human OSCC tissues from the TC and ITF were minced and digested in DMEM/F12 supplemented with 0.1% FBS (Invitrogen), 400 U/mL collagenase IV (Sigma), and 1% penicillin/streptomycin (Sigma) at 37 °C for 1 h. The suspension was centrifuged at 1000 rpm for 10 min and washed twice with DMEM/F12. The pellet was plated in 35-mm tissue culture dishes and incubated at 37 °C in 5% CO_2.

2.4 Proliferation assay

CAFs (1×10^4) isolated from the TC or ITF of WPOI1–3 or WPOI4–5 tumors were seeded in 96-well plates and cultured for 72 h. Cell proliferation was measured using the CellCounting-Lite 2.0 Luminescent Cell Viability Assay (Vazyme DD1101) and a microplate reader (Molecular Devices).

2.5 Transwell assay

2.5.1 CAFs migration assay

CAFs (3×10^5) from the TC or ITF of WPOI1–3 or WPOI4–5 tumors were added to the upper chamber of Transwell inserts, with 10% FBS medium in the lower chamber. After 24 h, non-migrated cells on the upper surface were removed, and migrated cells were fixed in formaldehyde for 20 min, stained with crystal violet for 10 min, and counted using ImageJ.

2.5.2 CAFs-induced OSCC cell migration assay

CAFs (3×10^5) were seeded in the lower chamber, and HN-6 cells (1×10^5) were placed in the upper chamber. After 24 h, migrated tumor cells were stained and counted as above.

2.6 RNA sequencing

Total RNA was extracted from paired TC- and ITF-derived CAFs obtained from patients A and D with WPOI1–3 tumors and patients B and E with WPOI4–5 tumors. For each patient, samples designated “-1” and “-2” represented the ITF and TC, respectively. RNA was isolated and sequenced by NovelBio. Sample B-2 was sequenced in two technical runs, which were combined before gene-level statistical analysis.

Raw reads were quality-filtered and adapter-trimmed using fastp and aligned to the human reference genome (GRCh38) using HISAT2. Gene-level counts were generated using HTSeq with Ensembl release 104 annotations. The raw sequencing data and gene-level count matrix have been deposited in the NCBI Gene Expression Omnibus (GEO) under accession number GSE349044.

Raw gene counts were analyzed using edgeR in R. Lowly expressed genes were removed using filterByExpr, and library sizes were normalized using the trimmed mean of M-values method. Gene-wise dispersions were estimated using robust estimation, and quasi-likelihood negative-binomial generalized linear models were fitted.

To account for the paired design, patient identity was included as a blocking factor. The model included patient, region and a WPOI-by-region interaction term. The interaction effect was defined as:

$(\text{ITF-TC})_{\text{WPOI4–5}}$-$(\text{ITF-TC})_{\text{WPOI1–3}}$.

Positive interaction $\log_2$ fold-change values therefore represented a greater TC-to-ITF increase in WPOI4–5 tumors than in WPOI1–3 tumors. Statistical significance was evaluated using quasi-likelihood F-tests, and P values were adjusted for multiple testing using the Benjamini–Hochberg procedure.

Because no individual interaction gene reached an FDR below 0.25, candidate interaction genes were considered exploratory. Exploratory candidates were prioritized on the basis of nominal interaction $P < 0.05$, absolute interaction $\log_2$

fold-change ≥1, absolute WPOI4–5 ITF-versus-TC $\log_2$ fold-change ≥1 and concordant changes in the two WPOI4–5 patient pairs.

For gene set enrichment analysis, genes were ranked using the signed square root of the quasi-likelihood F statistic, with the sign determined by the interaction $\log_2$ fold-change. Pre-ranked GSEA was performed using fgseaMultilevel and gene sets obtained from the Molecular Signatures Database through msigdbr. Hallmark, Reactome and Gene Ontology Biological Process gene sets containing 15–500 genes were included. Enrichment was summarized using the normalized enrichment score, and FDR-adjusted P values were reported. GSEA results were regarded as exploratory because of the limited number of biological samples.

2.7 Statistical analysis

Continuous data are expressed as mean ± SD. Paired comparisons (TC vs ITF within the same tumor) used paired t-tests; unpaired comparisons used unpaired two-tailed Student's t-tests. The region-by-WPOI interaction was assessed using a linear model with an interaction term, and the ITF–TC difference between WPOI groups was compared using a permutation test. Associations between α-SMA expression and clinicopathologic parameters were analyzed using the Pearson chi-square test or Fisher's exact test. Survival was analyzed by the Kaplan–Meier method with log-rank test. For transcriptomic data, A two-tailed $P < 0.05$ was considered statistically significant.

Results

1 CAFs are enriched at the ITF in WPOI4-5 OSCC

A total of 137 OSCC patients were enrolled in this study. To determine whether CAFs at the ITF or TC contribute to the WPOI formation, specimens were stratified by two experienced pathologists into a WPOI1-3 group (n = 59) and a WPOI4-5 group (n = 78).

IHC stain for α-SMA, a marker of CAFs, revealed strong staining in spindle-shaped cells (Fig1. A, B). In both WPOI1-3 and WPOI4-5 groups, α-SMA scores were significantly higher at the ITF than at the TC (both $P < 0.0001$), indicating a general center-to-front gradient of CAF activation (Fig1. C, D). Notably, this ITF-predominant pattern was more pronounced in WPOI4-5. The TC-to-ITF increase was significantly greater in WPOI4-5 (interaction $P = 0.0089$; Fig1. E), and the delta α-SMA score (ITF minus TC) was significantly larger in WPOI4-5 than in WPOI1-3 (permutation $P = 0.0088$; Fig1. F).

Together, these findings indicate that CAFs is more pronounced in ITF of WPOI4-5 OSCC, suggesting a higher correlation of WPOI4-5 and ITF-localized CAFs.

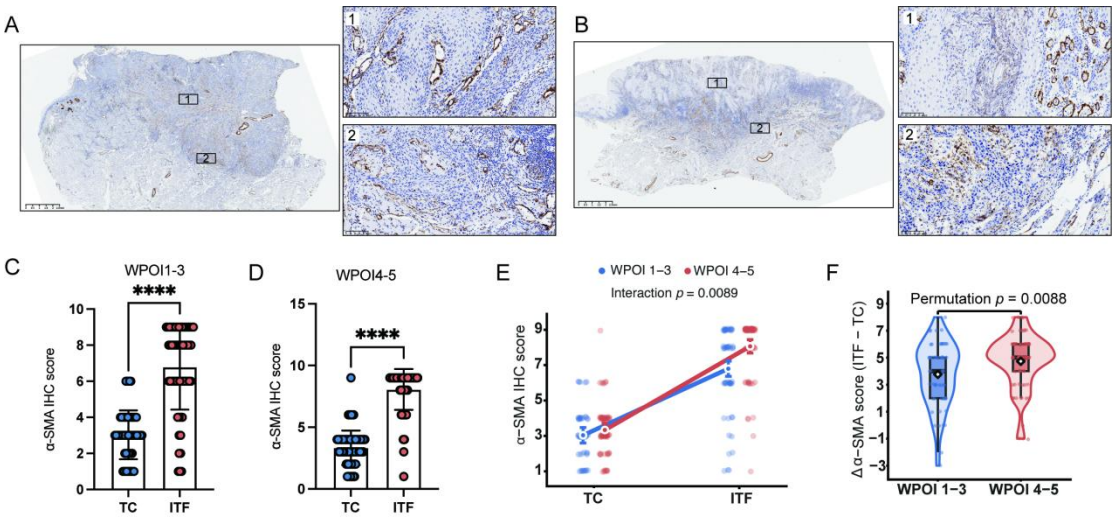


Figure 1 Distribution of α-SMA⁺ CAFs in the TC and ITF of WPOI1-3 and WPOI4-5 OSCC patients**.** (A, B) Representative IHC images of α-SMA staining in WPOI1-3 (A) and WPOI4-5 specimens (B). Left panels show whole-tumor scans; boxed regions 1 and 2 correspond to the TC and ITF, respectively, magnified in the right-hand panels. Scale bars are shown on each panel.

(C, D) Quantification of α-SMA IHC scores at the TC versus ITF in the WPOI1-3 group (C, n = 59) and WPOI4-5 group (D, n = 78). Each dot represents one patient; bars indicate mean ± SD. **** $P < 0.0001$.

(E) Comparison of the TC-to-ITF increase in α-SMA score between the WPOI1-3 (blue) and WPOI4-5 (red) groups. Lines connect group means at TC and ITF.

(F) Delta α-SMA score (Δα-SMA = α-SMA score at ITF minus α-SMA score at TC) compared between the WPOI1-3 and WPOI4-5 groups. Permutation test, P = 0.0088.

2 CAFs accumulation is associated with worse clinical outcomes specifically in WPOI4–5 OSCC

The above results indicate that CAFs is generally more pronounced at the ITF, and that this front enrichment is particularly evident in WPOI4-5 tumors. We then analyzed the relationship between α-SMA expression and clinicopathologic parameters at each location. Higher α-SMA expression in CAFs at the ITF was significantly associated with WPOI4–5 ($P<0.001$), whereas CAFs at the TC was not associated with WPOI but instead correlated with TNM stage (P=0.024) and depth of invasion (P=0.001). To test whether the within-patient front enrichment of α-SMA

was also associated with WPOI4–5, we analyzed the ITF–TC difference (Δα-SMA). Δα-SMA showed a trend toward association with WPOI4–5, although this did not reach statistical significance (P=0.093).

We then performed Kaplan-Meier analysis of α-SMA high and low CAFs at the TC and ITF, stratified separately within the WPOI1–3 and WPOI4–5 subgroups. Among WPOI1–3 tumors, α-SMA expression at neither the TC nor the ITF was associated with survival (Fig. 2A–B). In contrast, among WPOI4–5 tumors, high α-SMA expression at both the TC and the ITF was associated with significantly decreased OS (Fig. 2 C–D). Thus, although α-SMA$^+$ CAF accumulation at the ITF is specifically linked to the WPOI4–5 invasive pattern, the prognostic weight of α-SMA$^+$ CAF in WPOI4–5 tumors extends beyond the front to the tumor center, pointing to a field-wide stromal reprogramming in which the ITF represents the most functionally pronounced niche.

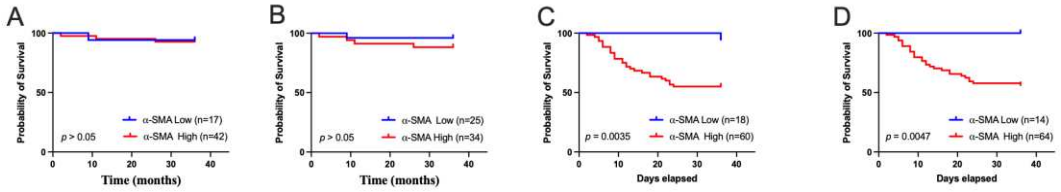


Figure 2. Kaplan–Meier survival analysis of α-SMA$^+$ CAF stratified by WPOI subgroup.

(A) Kaplan–Meier survival analysis of TC α-SMA expression in WPOI1–3 tumors.

(B) Kaplan–Meier survival analysis of ITF α-SMA expression in WPOI1–3 tumors.

(C) Kaplan–Meier survival analysis of TC α-SMA expression in WPOI4–5 tumors.

(D) Kaplan–Meier survival analysis of ITF α-SMA expression in WPOI4–5 tumors.

3 Transcriptional Features of ITF-Specific CAFs in WPOI4–5 Tumors

Given the preferential association of WPOI4–5 tumors with CAFs enrichment at the ITF, we next investigated the transcriptomic programs underlying region-specific CAFs in WPOI4–5 tumors. Paired CAFs were isolated from the TC and ITF of two WPOI1–3 patients (A and C) and two WPOI4–5 patients (B and D) and subjected to RNA sequencing. Gene expression was modeled as a function of WPOI status, tumor region, and their interaction. The interaction term captured the differential TC-to-ITF

expression shift between the two WPOI groups, formally defined as $(\mathrm{ITF} - \mathrm{TC})_{\mathrm{WPOI4–5}} - (\mathrm{ITF} - \mathrm{TC})_{\mathrm{WPOI1–3}}$.

No individual genes reached the prespecified FDR threshold, consistent with the constraints imposed by the limited sample size. We therefore adopted an exploratory analytical framework, prioritizing interaction candidates based on effect size, nominal statistical evidence, and concordance of expression changes across the two WPOI4–5 patients. Unsupervised hierarchical clustering of these candidate genes revealed substantial inter-patient heterogeneity. Nonetheless, the two WPOI4–5 ITF samples (B-1 and D-1) displayed relatively convergent expression patterns and co-clustered in this analysis (Fig. 3A). The genome-wide distribution of interaction effect sizes and nominal p-values is presented in Fig. 3B, with the exploratory candidate gene set highlighted for downstream analyses.

GSEA applied to the ranked interaction statistics identified positive enrichment of immune-regulatory and secretory programs, including interferon-gamma response, interferon-alpha response, inflammatory response, and complement activation. Interestingly, negative enrichment was observed for proliferative and metabolic programs, specifically E2F targets, MYC targets, G2M checkpoint, glycolysis, and oxidative phosphorylation (Fig. 3C). These findings collectively suggested that WPOI4–5 ITF-CAFs underwent a transcriptional shift toward inflammatory and secretory reprogramming, rather than reflecting a generalized increase in CAFs proliferative activity.

To further characterize the functional implications of this reprogramming, we performed a focused exploratory GO-GSEA restricted to gene sets related to tumor cell migration and extracellular matrix (ECM) regulation. Several ECM-remodeling and migration-related gene sets showed positive normalized enrichment scores, including regulation of extracellular-matrix organization and mesenchymal cell migration. However, negative regulation of locomotion was also positively enriched, and most migration-related gene sets did not remain significant after multiple-testing correction (Fig. 3D). Collectively, these results indicate altered migration- and matrix-regulatory transcriptional programs in WPOI4–5 ITF-CAFs.

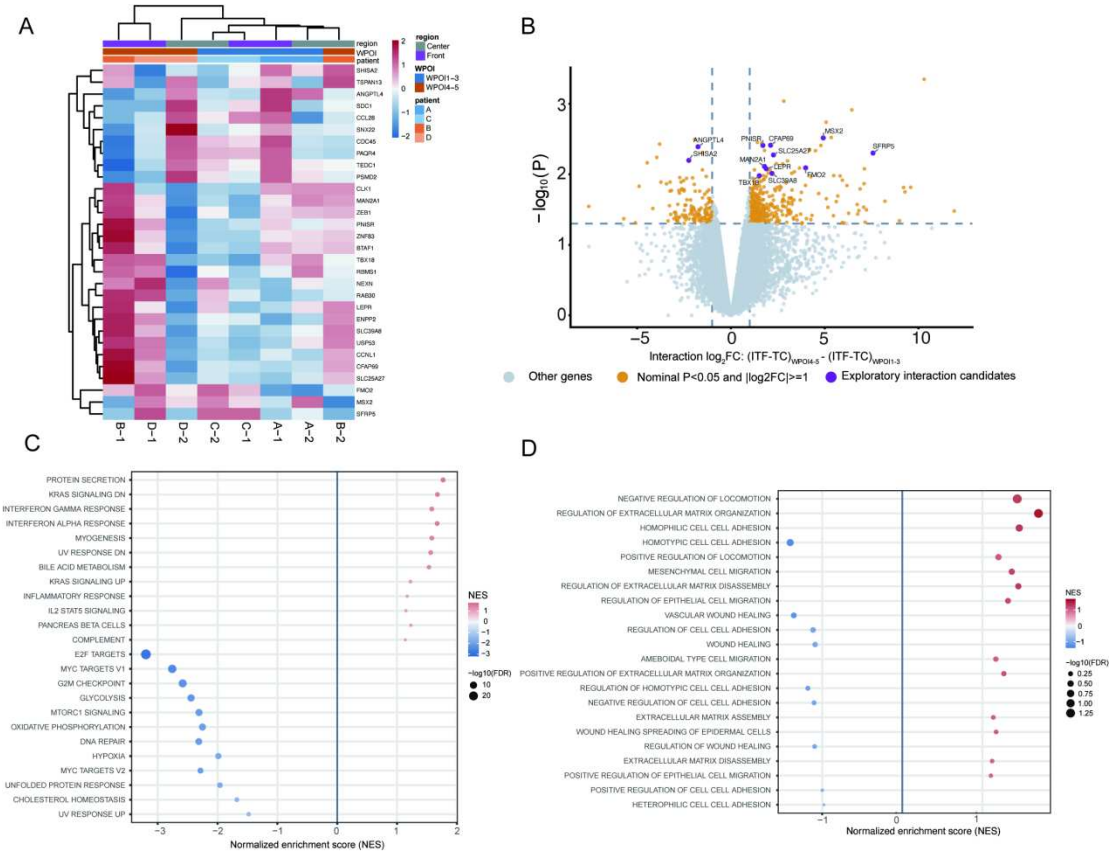


Figure 3 Paired transcriptomic interaction analysis identifies distinct transcriptional features of ITF CAFs in WPOI4–5 OSCC.

(A) Unsupervised hierarchical clustering of exploratory interaction candidate genes in paired CAFs isolated from the TC and ITF of WPOI1–3 and WPOI4–5 tumors. Expression values represent row-scaled, TMM-normalized $\log_2$ counts per million (CPM). Annotation bars indicate sampling region, WPOI group and patient identity.

(B) Volcano plot of the WPOI-by-region interaction effect, defined as $(\text{ITF-TC})_{\text{WPOI4–5}}$-$(\text{ITF-TC})_{\text{WPOI1–3}}$. The horizontal dashed line indicates nominal P=0.05, and the vertical dashed lines indicate |interaction log_2FC|=1. Orange points represent genes with nominal (P<0.05) and (|log_2FC| ≥1); purple points indicate exploratory interaction candidates selected according to interaction magnitude and concordant patient-level changes. No individual gene reached FDR<0.25.

(C) GSEA based on genes ranked by the signed interaction statistic. Positive NES indicate stronger TC-to-ITF enrichment in WPOI4–5 tumors, whereas negative NES values indicate stronger enrichment in WPOI1–3 tumors. Bubble color represents NES, and bubble size represents $-\log_{10}$(FDR).

(D) Focused GO GSEA of tumor-cell migration, cell adhesion and extracellular-matrix-regulation terms, after excluding immune-cell- and vascular-cell-specific migration pathways. Positive NES values indicate stronger TC-to-ITF enrichment in WPOI4–5 tumors. Bubble color represents NES, and bubble size represents $-\log_{10}$(FDR). These analyses were exploratory because the cohort comprised four patients with paired TC and ITF samples.

4 ITF-CAFs in WPOI4-5 displayed the strongest pro-migrating ability in vitro

To functionally validate the transcriptional reprogramming identified in WPOI4–5 ITF-CAFs, we assessed the proliferative capacity, migratory activity, and pro-tumorigenic function of CAFs isolated from the TC and ITF of WPOI1–3 and WPOI4–5 tumors.

Proliferation assays revealed no significant difference between TC- and ITF-derived CAFs within either WPOI group (Fig. 4A). However, CAFs from WPOI4–5 tumors exhibited significantly greater proliferative capacity compared to their WPOI1–3 counterparts, regardless of anatomical origin. This finding is consistent with the transcriptomic data showing negative enrichment of MYC targets and E2F targets specifically in WPOI4–5 ITF-CAFs relative to TC-CAFs, suggesting that the transcriptional suppression of proliferative programs at the ITF occurs against a background of globally elevated CAF proliferative potential in high-WPOI tumors.

Transwell migration assays demonstrated that ITF-derived CAFs migrated significantly more than TC-derived CAFs in both WPOI groups, with WPOI4–5 ITF-CAFs exhibiting the highest migratory capacity overall (Fig. 4B). This region-specific enhancement of CAF motility in WPOI4–5 tumors aligns with the positive enrichment of ECM-remodeling and mesenchymal cell migration gene sets observed in the interaction GSEA, supporting the functional relevance of these transcriptional alterations.

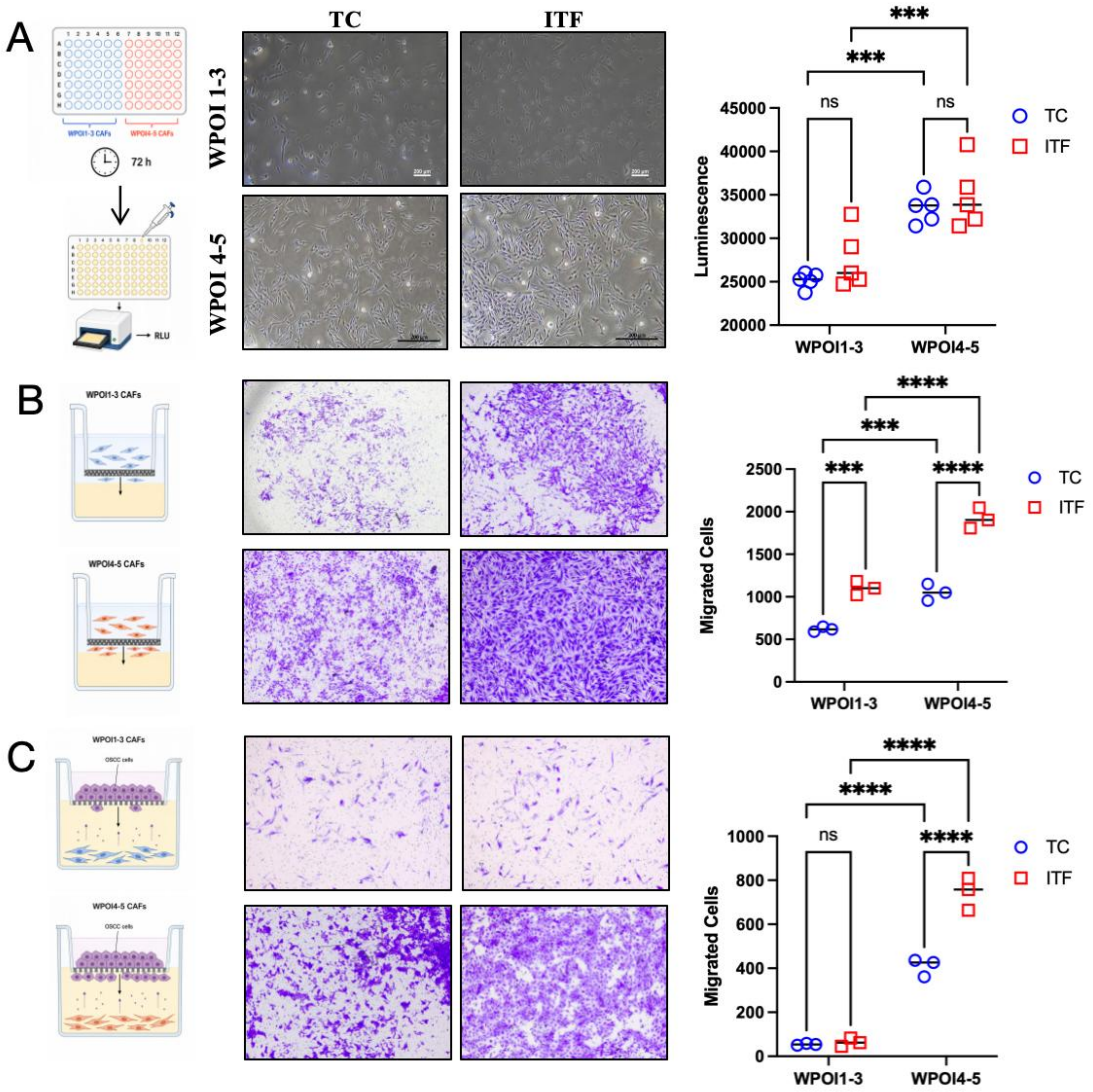


Figure 4 Functional characterization of CAFs derived from TC and ITF in WPOI1–3 and WPOI4–5 tumors.

(A) Proliferative capacity of CAFs isolated from the TC and ITF of WPOI1–3 and WPOI4–5 tumors was assessed by ATP-based luminescence assay after 72 hours of culture (Left). Representative phase-contrast images (Middle, scale bar, 200 μm) and quantification of relative luminescence units (Right, RLU) are shown. n = 5 per group. **(B)** Migratory ability of TC- and ITF-derived CAFs was evaluated by Transwell migration assay (Left). Representative crystal violet-stained images (Middle) of migrated cells and quantification of migrated cell counts (Right) are shown. n = 3 per group. **(C)** Pro-migratory paracrine activity of TC- and ITF-derived CAFs was assessed by co-culture Transwell assay using HN6 cell (Left). Representative images (Middle) and quantification of migrated HN6 cells (Right) are

shown. n = 5 per group. Statistical comparisons were performed by one-way ANOVA with post hoc testing. ***p < 0.001; ****p < 0.0001; ns, not significant.

Collectively, these in vitro findings demonstrate that WPOI4–5 CAFs, particularly those residing at the ITF, possess enhanced migratory, and tumor cell-promoting capacities compared to WPOI1–3 CAFs, providing functional corroboration for the transcriptional reprogramming and supporting a pro-invasive role for ITF-specific CAF activation in high-WPOI OSCC.

Discussion

In this study, we compared the abundance, spatial distribution, functional and transcriptional properties of CAFs between WPOI1-3 and WPOI4-5 tumors, at both the TC and the ITF. Consistent with previous reports that CAFs at the ITF drive tumor progression, we found that α-SMA-positive CAFs were enriched at the ITF relative to TC in both WPOI groups[17-19]. Notably, this front-to-center enrichment was significantly more pronounced in WPOI4-5 tumors. This indicates that spatial polarization of CAFs is not unique to WPOI4-5, but is amplified in this more invasive histological pattern.

Our results extend the growing recognition of CAFs heterogeneity. Single-cell studies have defined transcriptionally distinct CAF subtypes, including myofibroblastic (myCAF), inflammatory (iCAF), and antigen-presenting (apCAF) populations [20,21], and spatial transcriptomic approaches have begun to map location-dependent CAF diversity within tumors[20,22]. However, the spatial dimension of CAF heterogeneity across WPOI remained unexplored. By comparing CAFs isolated from the TC and ITF of WPOI1–3 and WPOI4–5 tumors, we provide functional evidence that the ITF of WPOI4–5 tumors harbors a CAF population with enhanced pro-tumor properties, thereby linking spatial CAF heterogeneity to a clinically defined invasive pattern.

A central question raised by our findings is the direction of causality between ITF CAFs and WPOI4–5 tumor cells. Two non-exclusive scenarios are plausible. On one hand, ITF CAFs may actively educate tumor cells toward a dispersed, non-cohesive invasive phenotype, consistent with our previous demonstration that CAFs promote WPOI4–5 formation through OXTR–ERK signaling[13]. On the other hand, the

observation that high α-SMA expression at both the TC and ITF predicted poor survival specifically in WPOI4–5 tumors, despite α-SMA expression in TC being unassociated with WPOI grade, suggests that WPOI4–5 tumor cells may impose a field-wide stromal reprogramming that extends beyond the invasive front. In this model, the ITF represents the site where this reprogramming is most functionally pronounced, owing to the intensity of tumor–stroma crosstalk at the tumor–host interface. Reciprocal co-culture systems and spatially resolved molecular profiling will be required to dissect this bidirectional interaction.

Stromal fibroblasts can influence tumor persistence and metastatic competence by establishing supportive tissue niches, indicating that tumor behavior is not determined by tumor-cell-autonomous mechanisms alone[23,24]. In OSCC, accumulating clinical evidence also links CAFs abundance to disease recurrence and unfavorable outcomes [10,25,26]. In the present study, α-SMA-positive CAFs were enriched at the ITF and were strongly associated with the WPOI4–5 invasive pattern. These findings raise the hypothesis that an activated stromal niche at or beyond the invasive front may contribute to postoperative recurrence, particularly in WPOI4–5 OSCC. However, because margin-specific CAFs abundance and recurrence-free survival were not evaluated in our cohort, this possibility cannot be established from the present data. Longitudinal studies incorporating spatial assessment of CAFs at the ITF and surgical margins, together with paired primary and recurrent tumors, are warranted to determine whether residual or persistent CAF programs are associated with local recurrence and whether they could inform surgical-margin assessment and adjuvant treatment.

Several limitations should be acknowledged. First, the transcriptomic analysis was based on a limited number of patient-derived CAF samples, and the interaction candidates identified require validation in larger, independent cohorts. Second, α-SMA was used as the primary CAF marker; although we complemented histological quantification with functional assays, the inclusion of additional markers (e.g., FAP, POSTN) and multiplex spatial profiling would provide a more refined characterization of CAF subtypes. Third, our in vitro assays, while informative, cannot fully recapitulate the spatial architecture and dynamic crosstalk of the tumor–stroma interface in vivo.

In summary, our study identifies ITF CAFs in WPOI4–5 OSCC as a functionally distinct population with the highest pro-tumor migratory capacity, and provides evidence that these cells may contribute to the formation of the WPOI4–5 invasive phenotype. Targeting this spatially defined CAF population, or the signaling pathways that sustain its pro-invasive function, may represent a promising therapeutic strategy for patients with highly invasive OSCC.

Funding:

The research is funded by Key Research and Development Projects in Jiangsu Province (No. BE2020628).

Author Contributions

Qingang Hu and Lei Zhang conceived the work; Qingang Hu acquired the funding; Lei Zhang was responsible for the methodology and analysis; Ting Zhou wrote the original draft; Xiaoxin Zhang edited the paper; Yanhong Ni supervised the work.

Data Availability Statement

The raw sequencing data and processed gene-count matrix generated in this study are publicly available in the NCBI GEO under accession number GSE349044. All other data supporting the findings of this study are available from the corresponding author upon reasonable request.

Competing interests

The authors declare no competing interests.

References

1 Tan, Y. *et al.* Oral squamous cell carcinomas: state of the field and emerging directions. *Int J Oral Sci* **15**, 44 (2023). https://doi.org:10.1038/s41368-023-00249-w

2 Taghavi, N. & Yazdi, I. Prognostic factors of survival rate in oral squamous cell carcinoma: clinical, histologic, genetic and molecular concepts. *Arch Iran Med* **18**, 314-319 (2015).

3 Brandwein-Gensler, M. *et al.* Oral squamous cell carcinoma: histologic risk assessment, but not margin status, is strongly predictive of local disease-free and overall survival. *Am J Surg Pathol* **29**, 167-178 (2005). https://doi.org:10.1097/01.pas.0000149687.90710.21

4 Johnson, D. E. *et al.* Head and neck squamous cell carcinoma. *Nat Rev Dis Primers* **6**, 92 (2020). https://doi.org:10.1038/s41572-020-00224-3

5 Beute, J. E. *et al.* WPOI-5: Accurately Identified at Intraoperative Consultation and Predictive of Occult Cervical Metastases. *Head Neck Pathol* **17**, 479-486 (2023). https://doi.org:10.1007/s12105-023-01533-1

6 Binmadi, N. O. & Mohamed, Y. A. Impact of worst pattern of invasion on prognosis of oral squamous cell carcinoma: a systematic review and meta-analysis. *J Int Med Res* **51**, 3000605231206260 (2023). https://doi.org:10.1177/03000605231206260

7 Mishra, A. *et al.* Worst pattern of invasion in oral squamous cell carcinoma is an independent prognostic factor. *J Oral Biol Craniofac Res* **12**, 771-776 (2022). https://doi.org:10.1016/j.jobcr.2022.08.027

8 Togni, L. *et al.* Prognostic Role of Worst Pattern of Invasion in Oral Squamous Cell Carcinoma. *J Clin Med* **15** (2026). https://doi.org:10.3390/jcm15030965

9 Shete, M. V. *et al.* Prognostic Ability of Expression of Myofibroblasts in Oral Squamous Cell Carcinoma: A Systematic Review and Meta-Analysis. *Asian Pac J Cancer Prev* **25**, 1477-1486 (2024). https://doi.org:10.31557/APJCP.2024.25.5.1477

10 Dourado, M. R., Guerra, E. N. S., Salo, T., Lambert, D. W. & Coletta, R. D. Prognostic value of the immunohistochemical detection of cancer-associated fibroblasts in oral cancer: A systematic review and meta-analysis. *J Oral Pathol Med* **47**, 443-453 (2018). https://doi.org:10.1111/jop.12623

11 Kunhikannan, A., Suresh, T. N. & Mohiyuddin, S. M. A. A Study on Cancer-Associated Fibroblast Using Alpha-Smooth Muscle Actin Immunohistochemistry in Oral Squamous Cell Carcinoma. *Cureus* **17**, e85027 (2025). https://doi.org:10.7759/cureus.85027

12 Sutera, S., Furchi, O. A. & Pentenero, M. Exploring Cancer-Associated Fibroblasts in OSCC and OPMDs: Microenvironment Insights. Scoping Review. *Oral Dis* **31**, 1982-1990 (2025). https://doi.org:10.1111/odi.15275

13 Ding, L. *et al.* OXTR(High) stroma fibroblasts control the invasion pattern of oral squamous cell carcinoma via ERK5 signaling. *Nat Commun* **13**, 5124 (2022). https://doi.org:10.1038/s41467-022-32787-y

14 Biffi, G. & Tuveson, D. A. Diversity and Biology of Cancer-Associated Fibroblasts. *Physiol Rev* **101**, 147-176 (2021). https://doi.org:10.1152/physrev.00048.2019

15 Yamamoto, Y. *et al.* The heterogeneity of cancer-associated fibroblast subpopulations: Their origins, biomarkers, and roles in the tumor microenvironment. *Cancer Sci* **114**, 16-24 (2023). https://doi.org:10.1111/cas.15609

16 Chhabra, Y. & Weeraratna, A. T. Fibroblasts in cancer: Unity in heterogeneity. *Cell* **186**, 1580-1609 (2023). https://doi.org:10.1016/j.cell.2023.03.016

17 He, J. Z. *et al.* Spatial analysis of stromal signatures identifies invasive front carcinoma-associated fibroblasts as suppressors of anti-tumor immune response in esophageal cancer. *J Exp Clin Cancer Res* **42**, 136 (2023). https://doi.org:10.1186/s13046-023-02697-y

18 Jin, W. *et al.* HAS1(high) cancer associated fibroblasts located at the tumor invasion front zone promote oral squamous cell carcinoma invasion via ECM remodeling. *J Exp Clin Cancer Res* **44**, 238 (2025). https://doi.org:10.1186/s13046-025-03493-6

19 Garcia-Rodriguez, J. L. *et al.* Cancer-associated fibroblasts shape the formation of budding cancer cells at the invasive front of human colorectal cancer. *Commun Biol* **8**, 1345 (2025). https://doi.org:10.1038/s42003-025-08799-x

20 Elyada, E. *et al.* Cross-Species Single-Cell Analysis of Pancreatic Ductal Adenocarcinoma Reveals Antigen-Presenting Cancer-Associated Fibroblasts. *Cancer Discov* **9**, 1102-1123 (2019). https://doi.org:10.1158/2159-8290.CD-19-0094

21 Flynn, J. M. *et al.* Plasticity and Functional Heterogeneity of Cancer-Associated Fibroblasts. *Cancer Res* **85**, 3378-3398 (2025). https://doi.org:10.1158/0008-5472.CAN-24-3037

22 Wang, Q. *et al.* Spatially Resolved Transcriptomics Technology Facilitates Cancer Research. *Adv Sci (Weinh)* **10**, e2302558 (2023). https://doi.org:10.1002/advs.202302558

23 Skrupskelyte, G. *et al.* Precancerous niche remodelling dictates nascent tumour persistence. *Nature* **653**, 242-253 (2026). https://doi.org:10.1038/s41586-026-10157-8

24 Buissant des Amorie, J. R. *et al.* Emergence of oncofetal plasticity is ubiquitous in early colorectal cancers. *Nature* **654**, 229-239 (2026). https://doi.org:10.1038/s41586-026-10344-7

25 Vered, M., Shnaiderman-Shapiro, A., Zlotogorski-Hurvitz, A., Salo, T. & Yahalom, R. Cancer-associated fibroblasts in the tumor microenvironment of tongue carcinoma is a heterogeneous cell population. *Acta Histochem* **121**, 151446 (2019). https://doi.org:10.1016/j.acthis.2019.151446

26 Haga, K. *et al.* Crosstalk between oral squamous cell carcinoma cells and cancer-associated fibroblasts via the TGF-beta/SOX9 axis in cancer progression. *Transl Oncol* **14**, 101236 (2021). https://doi.org:10.1016/j.tranon.2021.101236

Supplementary Files

This is a list of supplementary files associated with this preprint. Click to download.

- table.xlsx